Material Contrast of Scanning Electron and Ion Microscope Images of Metals

T. Suzuki[a], M. Kudo[a], Y.Sakai[a], and T. Ichinokawa[b]
[a]JEOL Ltd., 3-1-2, Musashino, Akishima, Tokyo 196-8558 Japan
[b]Waseda University, Okubo, Shinjuku-ku, Tokyo Japan
ichinokawa@kurenai.waseda.jp

CrossMark

https://doi.org/10.1017/S1551929500054250 Published online by Cambridge University Press

Introduction

The rapid technical development of FIM (Focused Ion Beam) technology has spawned an increase in spatial resolution capability in scanning ion microscopy (SIM) technology[1]. Furthermore, FIM has been used for preparation of thin specimens in transmission electron microscopy[2] and micro-fabrication of electronic devices in the semiconductor industry[3]. Recently, a scanning ion microscope with a helium field ion source has been developed[4]. Thus, the contrast formation of emission electron images in scanning ion microscopy has been the object of study for analyzing images of materials specimens, similar to the theory behind scanning electron microscope (SEM) contrast formation[5,6,7]. Furthermore, whether the electron emission yield γ induced by ion impact is periodic or non-periodic as a function of Z_2 (the atomic number of the target) has not been well studied in the low energy region from several keV to the several tens of keV values used in SIM. Thus, in the present article, comprehensive experiments on γ as a function of atomic number Z_2 and the electronic structures of target metals have been performed for a number of metals for incident beams of 10 keV electron, 3 keV Ar^+- and 30 keV Ga^+-ions. The Z_2 oscillation of γ shows the anti-phase relationship between electron and Ar^+-ion impact and a different behavior for Ga^+-ion impact. The origins of these effects are discussed based on different mechanisms of electron emission for these projectiles.

Experiment

One of the tools used in this experiment is a scanning Auger electron microscope (JAMP-7800F) with a back pressure of 7×10^{-8} Pa installed with a hemi-spherical electron energy analyzer, a secondary electron detector system, consisting of a scintillator and a photo-multiplier tube, and an Ar^+-ion gun with a beam diameter that is variable from 0.1 to several mm. The other tool used is a scanning Ga^+-ion microscope (Micron-9000) with a detector system composed of an annular micro-channel plate ,which is mounted coaxially with the incident beam and can be biased for detecting either positive or negative particles. Secondary electron yields are, in general, far larger than those of the secondary negative ions, so negative particle imaging is essentially electron imaging. The energies of the electron and Ar^+ ion beams of the JAMP-7800F were 10 keV and 3 keV, respectively, and the energy of Ga^+-ion beam of the Micron-9000 was 30 keV.

Secondary electron yields were measured from the integrated intensities of the secondary electron spectra in an energy range from 0 to 30 eV for the JAMP-7800 and from the output signals of the micro-channel plate for the Micron-9000. The secondary electron yields obtained in this study are therefore relative values in each experiment, because the experimental arrangements of the secondary electron detectors differ.

Experimental results

Strips of several metal films of 1μm thickness and 0.1~1 mm width were deposited on a Si(100)2×1 clean surface in the order of Z_2. The target films were Al, Cu, Ag, and Au metals with a similar

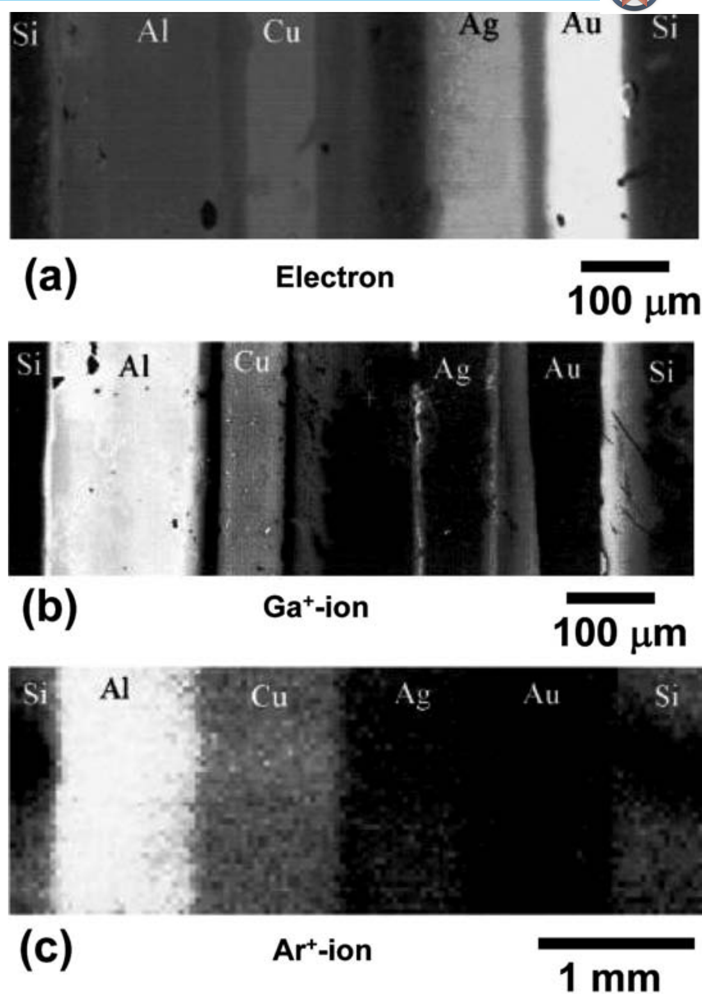

Fig. 1 Scanning images of samples of Al, Cu, Ag, and Au strip films deposited on Si clean surfaces; (a) a secondary electron image by 10 keV electrons, (b) an electron emission image by 30 keV Ga^+-ion, and (c) an electron emission image by 3 keV Ar^+-ion. The contrast changes with Z_2 dependent on the type of projectiles are discussed in the text. .

electronic structure. Fig.1(a) shows the secondary electron image obtained by the JAMP-7800F using a 10 keV electron beam. Brightness increases with Z_2. Whereas Fig.1(b) shows the secondary electron image obtained by the Micron-9000 using a Ga^+-ion beam at 30 keV and shows the brightness decreasing with increasing Z_2. Fig.1(c) shows the secondary electron image obtained by the JAMP-7800F using an Ar^+-ion beam at 3 keV and the brightness decreases with increasing Z_2 similar to that of the Ga^+-ion impact.

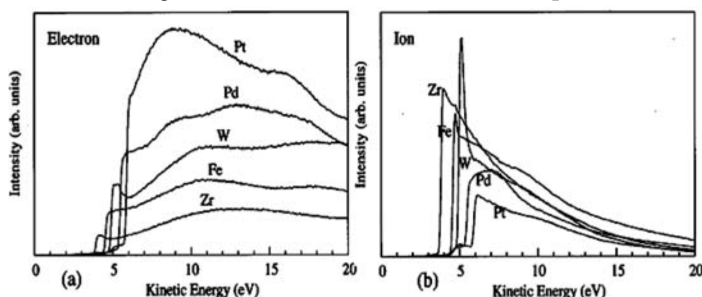

Fig. 2 Secondary electron spectra obtained by (a) 10 keV electrons, and (b) 3 keV Ar^+-ions for several metals. A bias potential -5 V was applied to the samples. The order of magnitude of the integrated intensities for the secondary electron spectra for the metals are opposite between electron and ion impact. On the other hand, the work function Φ measured from the onset energies of the secondary electron spectra shows the same values between electron and Ar^+-ion impact.

OmniGIS™
HWY
IN THE WOODS
OUT OF GAS
UP THE CREEK
SINGLE SOURCE CIR.
NO FEEDBACK LN.
OUT OF PORTS BLVD.

Get There With the OmniGIS™

The **NEW OmniGIS™** provides an economical, smart and flexible platform for routine processes as well as for the exploration of innovative gas chemistries in the SEM or FIB.

The OmniGIS™ features:

- Three on-board precursors
- Single needle delivery
- Two external carrier/purge gas inputs
- Gas flow feedback control
- Programmable process flows

User-replaceable sources reduce downtime.
Multiple gases on one port expand options.
Feedback control supports automation.

Omniprobe
www.omniprobe.com

https://doi.org/10.1017/S1551929500054250 Published online by Cambridge University Press

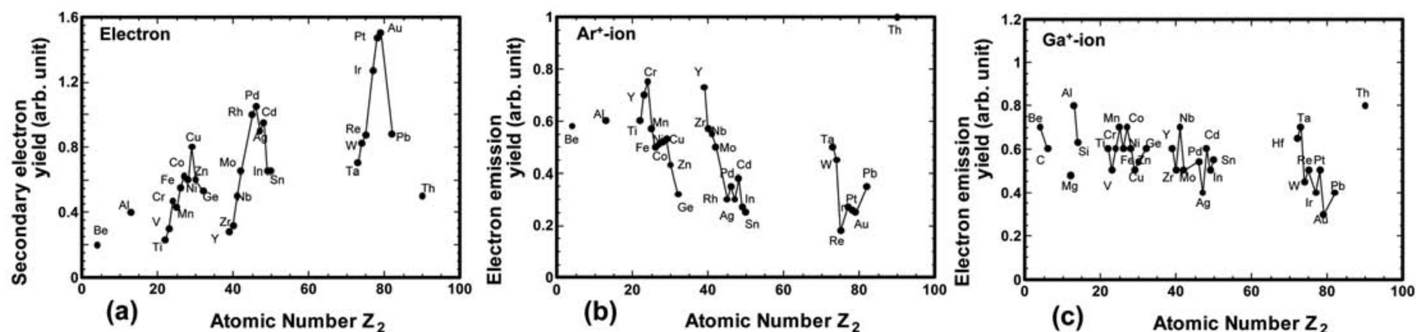

Fig. 3 Z_2 dependences of the secondary electron yield γ for (a) 10 keV electron, (b) 3 keV Ar^+-ion, and (c) 30 keV Ga^+-ion impact. The Z_2 oscillations are the anti-phase between electron and Ar^+-ion impact and the behavior of Ga^+-ion impact is different from those of electron and Ar^+-ion impact.

On the other hand, the Z_2 dependences of γ for 30 different metals were measured using incident beams of 10 keV electron, 3 keV Ar^+-ion and 30 keV Ga^+-ions. The specimens are polycrystalline pure metals prepared by Geller Analytical Laboratory. The secondary electron spectra obtained by the hemi-spherical electron energy analyzer are shown in Fig.2(a) and (b) for incident beams of 10 keV electron and 3 keV Ar^+-ions. A bias potential of -5 V was applied to the specimens. The order of magnitude of the integrated intensities among the metals are opposite between electron and Ar^+-ion impact. On the other hand, the values of the work function Φ measured by the onset energies of the secondary electron spectra are almost the same between electron and Ar^+-ion impact.

Fig.3(a) shows the Z_2 oscillation of γ for 30 species of metals for 10 keV electrons. We can observe three peaks at approximately Z_2 = 30, 50 and 80 and three minima at positions of alkali metals. On the other hand, for Ar^+-ion impact in Fig. 3(b) the Z_2 oscillation is almost the anti-phase of that of the electron impact and γ decreases with increasing Z_2. The peaks of γ in the Ar^+-ion impact locate at valleys of the electron impact. Fig.3 (c) shows a relationship between γ and Z_2 for Ga^+-ion impact but the oscillation is not as clear as it was for the electron and Ar^+-ion impact.

Fig.4 shows the Z_2 oscillation of Φ obtained from the electron emission spectra. The oscillation of Φ measured in this experiment agrees with that of Table [8] measured by other methods. Here, we should notice that the Z_2 oscillation of Φ in Fig.4 shows a similar oscillation to that of γ for electron impact, but is anti-phase of that for Ar^+-ion impact. This fact indicates that the relationships between γ and Φ are opposite for electron and Ar^+-ion impact and different again from that of Ga^+-ion impact. Fig.5 (a)-(c) show the relationships between γ and Φ for three projectiles. The data are largely scattered by the effects of other parameters, however we can recognize that γ increases with Φ in (a), decreases with increasing Φ in (b), and has no correlation with Φ in (c). The different dependencies between γ and Z_2 and γ and Φ among the three projectiles is discussed in the next section.

Discussion

The mechanisms of electron emission induced by charged particles are not simply dependent on the type of projectiles and energy as described by Hasselkamp[9]. The process is divided into two types; (1) kinetic emission (KE) and (2) potential emission (PE). The potential emission does not require any kinetic energy for the projectile and is often dominant at very low impact energies—less than several eV [10,11]. For kinetic emission, there is a threshold velocity V_{th} to emit a conduction electron into the vacuum. The threshold velocity to eject a Fermi-electron with a velocity of V_F (~$1x10^6$ m/s) from the solid to the vacuum is calculated by the following equation[12,13,14] and approximately 1 keV for He^+-ion, 10 keV for Ar^+-ion and 30 keV for Ga^+-ion.

$$V_{th}=(1/2)V_F[(1+W/E_F)1/2 - 1] , \qquad (1)$$

where W and E_F are the work function and the Fermi energy of target metal.

For energies higher than the threshold, electrons can be emitted by direct energy transfer due to the collisions between projectiles and conduction electrons and this process is called "electron Kinetic Emission", eKE. Sternglass. [15] Baragiola *et al.*[12,13] presented semi-empirical equations for eKE. According to their equations , γ is a function of three factors; (1) an inelastic stopping power $(dE/dx)_e$ of the projectile[16], (2) the mean free path of the liberated electrons in a solid, and (3) an escape probability of the librated electrons from the surface into the vacuum. All three processes depend on the material's parameters in different respects. Therefore, it is impossible to express γ as a function of one parameter and the γ of the cascade process should be calculated by Monte Carlo simulation [17].

For eKE, the stopping power S_e is the most important factor and is related to the number density, N [16]. Furthermore, for metals S_e relates to the electron density of conduction band n, and connects to the Fermi energy E_F and the work function Φ. Such correlations were already pointed out by Baroody[18] and Dekker[19] a half-century ago and they showed theoretically that γ for electron impact is proportional to $E^{½}_F$ or $Φ^{½}$. In the present experiment, however, we found that γ for electron impact increases roughly with Φ as shown

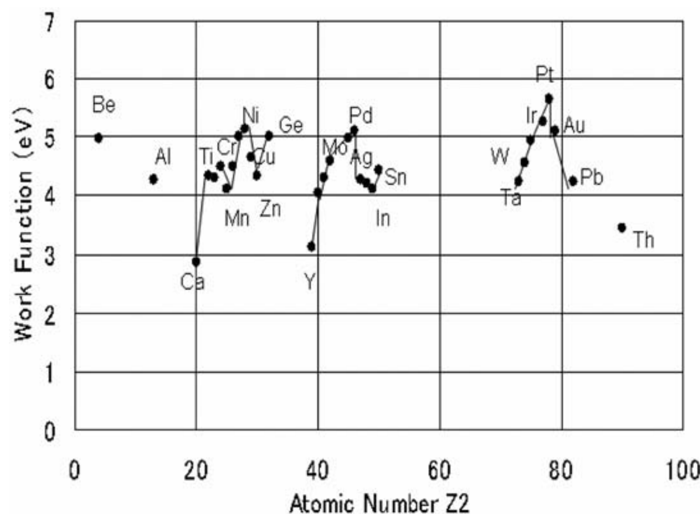

Fig.4 The relationship between the work function Φ and Z_2 obtained by this experiment. The data agree with Table [8]. The Z_2 oscillation of Φ is similar to that of γ for electron impact.

https://doi.org/10.1017/S1551929500054250 Published online by Cambridge University Press

Let 4pi take you beyond the capability of any SEM/STEM on the market with

RevolutionEDX

X-ray Microanalysis Systems optimized for productivity & ease of use

- Silicon-drift technology detectors
  - Liquid Nitrogen-free
  - High-throughput
  - 10 or 30 mm^2 sensor
- Work over a network via Gigabit Ethernet
- Easy to use: one-click acquisition for spectra, images, maps, spot probes and line scans
- Dynamic Dwell Modulation™ – spend maximum time on areas of interest while continuing to obtain x-ray data from the entire area
- Robust auto peak-ID based on real-time full deconvolution of acquired x-ray spectra

High resolution: 129eV or better
Super-ultra-fast spectrum imaging

Unique features save time & production costs

Event-Streamed Spectrum Imaging™
Collect x-ray spectrum images at electron imaging speeds

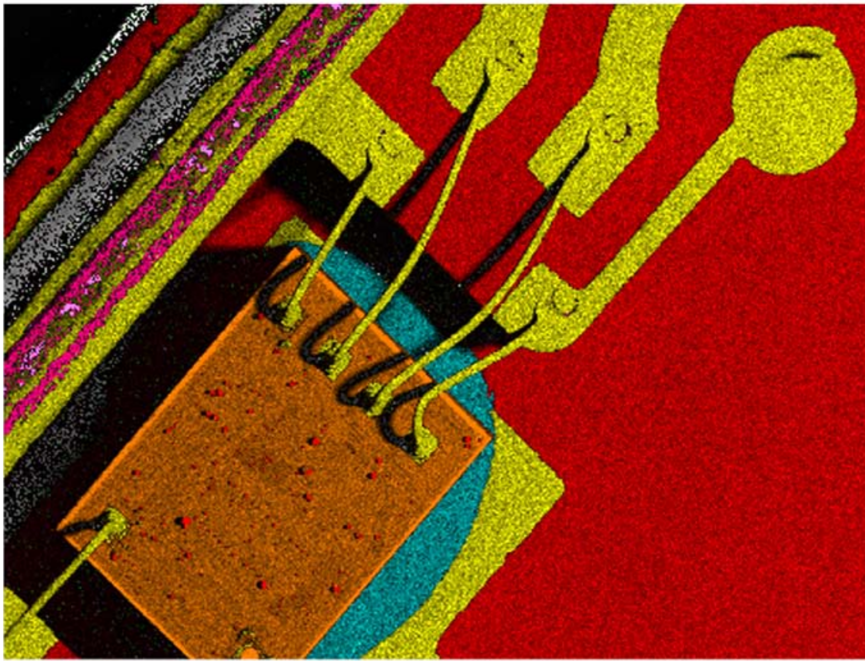

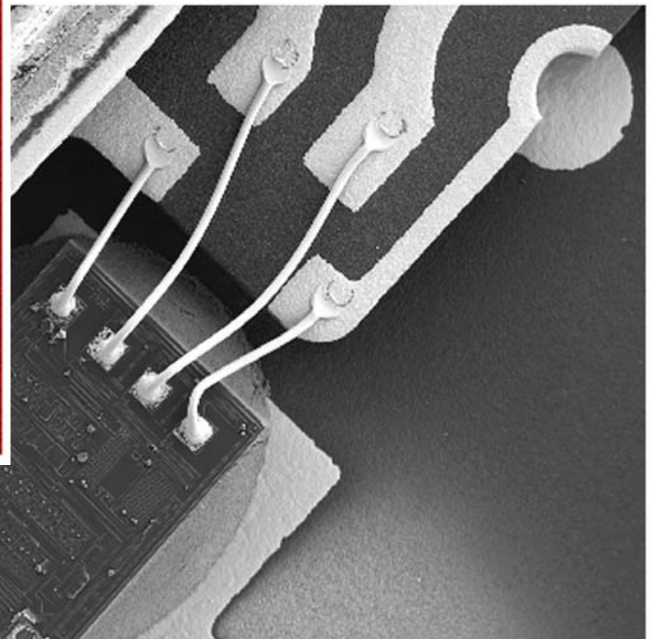

Spatial Frame Lock™
Real-time electron-beam drift correction

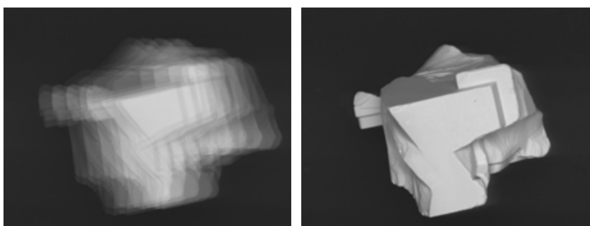

Available TODAY only from

www.4pi.com • sales@4pi.com
4pi Analysis, Inc. 919.489.1757

https://doi.org/10.1017/S1551929500054250 Published online by Cambridge University Press

https://doi.org/10.1017/S1551929500054250 Published online by Cambridge University Press

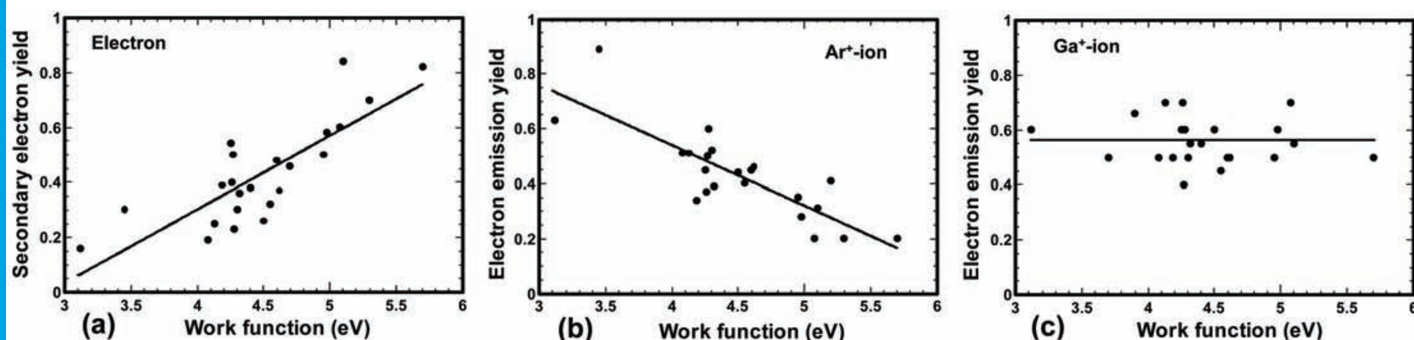

Fig.5 The relations between γ and Φ, (a)electron impact, (b) Ar^+-ion impact , and (c) Ga^+-ion impact. The data are largely scattered, but γ increases with Φ in (a), decreases with increasing Φ in (b), and shows no correlation with Φ in (c).

in Fig.5(a) based on the electron density of the target metal. This correlation seems to be contrary to common knowledge on electron emission when only considering escape potential.

Z_2 oscillation similar to the present experiment for electron impact was observed for H^+, H_2^+, and H_3^+ ion impacts at 100 keV/proton for 27 species of metals in ultrahigh vacuum by Hippler *et al* [20] and recently in helium ion microscopy at 20 keV by Morgan *et al.*[4]. These facts indicate that the electron emission mechanism by particles with high velocities is originated by eKE.

For Ar^+-ion impact, the projectile energy in this experiment is lower than the threshold, therefore electrons cannot be emitted by eKE. In this case, the most probable mechanism may be PE. The ionization potential of the Ar^+-ion, I_i , is 16 eV, therefore electrons can be emitted by an Auger neutralization process. As to PE, Kishinevskii[21] and Baragiola[22] reported that emission yield γ is proportional to the maximum emission energy, I_i-2Φ. Thus, we make a graph of I_i-2Φ *vs.* Z_2 and show it in Fig. 6. The Z_2 oscillation of Fig. 6 is similar to that of Fig.3 (b) and is anti-phase to that of the electron impact. This fact proves that the electron emission by Ar^+-ion impact is mainly caused by PE.

On the other hand, in Ga^+-ion impact at 30 keV, the projectile energy is comparable to the threshold and the ionization potential of the Ga^+ ion is 6 eV. This value is less than 2 Φ for a lot of metals. Therefore, electron emission is impossible by PE. As to the electron emission induced by ions with low energies and low ionization potentials, two mechanisms were proposed in KE.[23]

(1) The creation of the quasi-molecules composed of the projectile and the target atom in which some electronic levels may be strongly promoted to higher orbital energies and thus gives rise to electron emission in the subsequent de-excitation steps. This excitation mechanism is called "promotion Kinetic Emission", pKE. [24, 25]

(2) The excitation of the localized valence band electrons at the surface due to ion-electron collisions with the sub-threshold energy [26,27].

For electron emission in (2), γ shows the smooth exponential decay toward the low energy side caused by the smoothing of the surface potential and the decrease of the surface barrier less than Φ by means of interactions between projectiles and valence band electrons. This mechanism was labeled as "surface-assisted Kinetic Emission", sKE.[23]

In Fig.3(c) for Ga^+-ion impact, the peak positions are not clear, therefore the determination of the electron emission mechanism is impossible only from the Z_2 oscillation. The peak positions of e-KE exist approximately at 30, 50, and 80, while Z_2 positions where the outermost *p*-levels of the target atoms match with the electron levels of the projectiles may be shifted largely from the Z_2 positions of e-KE. Hofer *et al.*[28] measured the shift of Z_1 (atomic number of the projectile) oscillation for different metals and insisted that the maxima of the oscillatory structures were related to the level-matching of the quasi-molecular promotion. This occurrence strongly supports pKE. However, by our experiments, at energies from 1keV to 30 keV, γ for Ga^+-ion impact decreases continuously with projectile energy and there is no cut off energy on the low energy side. Since the kinetic energy of the projectile for pKE must be several keV for the promotion of quasi-molecules [23], it is reasonable to consider that the main process of electron emission for Ga^+-ion impact is to be s-KE.

For electron emission induced by ions with sub-threshold energies, several papers reported that calculated values of the threshold energies are higher than those of the experiment[29] and practical potential barriers across the surface are lower than the work function[30]. The mechanisms of Z_2 oscillation for projectiles with sub-threshold energies are very complicated and cannot be decided from the Z_2 oscillation only. Thus, we can understand that the identification of materials from the contrast observed in the scanning Ga^+-ion microscope images is very difficult compared to those of SEM images. A number of papers were published in the last decade on the study of electron emission induced by particles, however no full explanation of the observed Z_2 oscillations is available at present. Measurements of γ for ion impact at low energies are lacking, but would be of considerable interest. The projectiles and

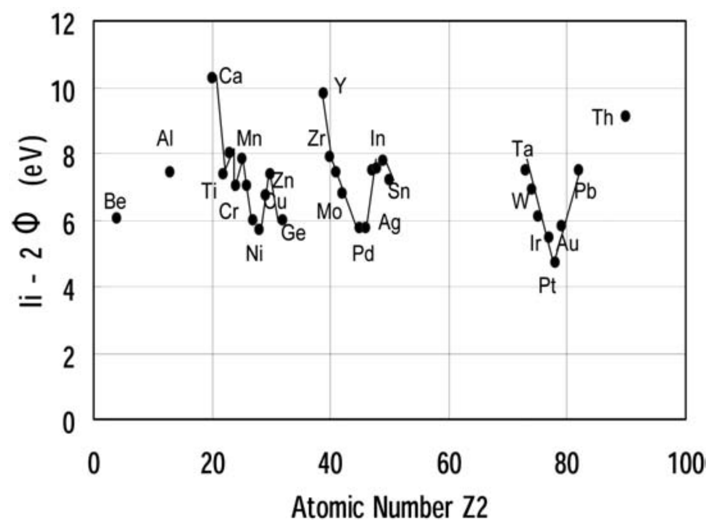

Fig.6 The values of Ii – 2Φ are plotted as a function of Z_2. The Z_2 oscillation of Ii –2Φ is similar to that of Fig.3(b). This fact implies that γ for Ar^+-ion impact is caused by PE.

energies used in this experiment were chosen arbitrarily, therefore the fact that all mechanisms of the three projectiles are different from each other is accidental.

Conclusion

Contrast mechanisms of scanning electron and ion microscope images for metals are studied for projectiles of 10 keV electron, 3 keV Ar^+-ion, and 30 keV Ga^+-ions. The Z_2 dependence of γ shows that different behaviors depending on the type of projectiles and energies occur. For electron impact, the emission is caused by e-KE and γ increases with the density of the valence band electrons and increases roughly with Φ or the electron negativity of the metal [31]. While for Ar^+-ion impact, electron emission is caused by PE and the relationships between γ and Z_2 and γ and Φ are opposite to those for electron impact. For Ga^+-ion impact, these relationships are not as distinct as those for electron and Ar^+-ion impact and the most reliable mechanism for Ga^+-ion impact may be s-KE.

Lastly, we would like to suggest that an investigation of the Z_2 oscillation of γ is one of the most important factors to study to pin down the mechanism of electron emission dependencies on the type and energies of projectiles. ■

References:

(1) R. Levi-Setti, *Scanning Electron Microscopy* 1, 1 (1983).
(2) T. Ishitani, H. Tsuboi, T. Yaguchi, H. Koike, *J. Elect. Microsc.* 43, 322 (1994).
(3) R.L. Seliger, R.L. Kubena, R.D. Olney, J.W. Ward, and V. Wang, *J. Vac. Sci. Tech.* 16, 1610 (1979); J. Melngailis, *J. Vac. Sci. Tech.* B5, 469 (1987).
(4) J. Morgan, J. Notte, R. Hill, and B. Ward, *Microscopy Today* 14, 24 (2006).
(5) Y. Sakai, T. Yamada, T. Suzuki, T. Sato, H. Itoh and T. Ichinokawa, *Appl. Phys. Lett.* 73, 611 (1998).
(6) M. Kudo, Y. Sakai and T. Ichinokawa, *Appl. Phys. Lett.* 76, 3475 (2000).
(7) T. Suzuki, N. Endo, M. Shibata, S. Kamasaki and T. Ichinokawa, *J. Vac. Sci. Tech.* A22, 49 (2004).
(8) H.B. Michaelson, *J. Appl. Phys.* 48, 4729 (1977).
(9) D. Hasselkamp, Particle Induced Emission II 123, 1-95 (Springer, Berlin, 1991)
(10) H.D.Hangstrum, In Electron and Ion Spectroscopy of Solids, edited by L. Fiermans, J. Vennik and D. Dekeyser (Plenum, New York, 1978).
(11) H.D. Hangstrum, *Phys. Rev.* 89, 244 (1953).
(12) R.A. Baragiola, E.V. Alonso and A. Oliva-Florio, *Phys. Rev. B* 19, 121 (1979).
(13) R.A. Baragiola, E.V. Alonso, J. Ferron and A. Oliva-Florio, *Surf. Sci.* 90, 240 (1979).
(14) E.V. Alonso, R.A. Baragiola, J. Ferron, M.N. Jakas and A. Oliva-Florio, *Phys. Rev. B* 22, 80 (1980)
(15) E.J. Sternglass, *Phys. Rev.* 108, 1 (1957).
(16) H. A.Bethe, *Phys. Rev.* 59, 940 (1941).
(17) T. Ishitani, Y. Madokoro, M. Nakagawa and K. Ohya, *J Electron Microscopy* 51, 207 (2002).
(18) E.M. Baroody, *Phys. Rev*. 108, 780 (1950).
(19) J. Dekker, Solid State Physics (Prentice-Hall, Englewood Cliffs, N.Y. 1957), Chap.17.
(20) S. Hippler, D. Hasselkamp and A. Scharmann, Nucl. Instrum. Methods, in *Phys. Res. B* 34, 518 (1988).
(21) L.M. Kishinevskii, *Rad. Effects* 19, 23 (1973).
(22) R.A. Baragiola, *Surf. Sci.* 90, 240 (1979).
(23) J. Lörincik, Z. Šroubek, H. Eder. F. Aumayr and H. Winter, *Phys. Rev. B* 62 , 16116 (2000).
(24) M.Barat and W. Lichten, *Phys. Rev. A* 6, 211 (1972).
(25) U. Wille and R. Hippler, *Phys. Rep*. 132, 129 (1986).
(26) J. A. Yarmoff, T. D. Liu, S. R.Qiu, and Z. Sroubeck. *Phys. Rev. Lett.* 80, 2469 (1998).
(27) G. Lakits, F. Arnau, and HP. Winter, *Phys. Rev. A* 42, 15 (1990).
(28) M.M. Ferguson and W.O. Hofer, *Rad. Effects and Defects in Solids*, 109, 273 (1989).
(29) H. Eder, W. Messerschmidt, HP. Winter, and F. Aumayr, *J. Appl. Phys.* 87, 8198 (2000).
(30) J. Lörincik, and Z. Šroubek, Nucl. Instrum. Methods *Phys. Res. B* 164-165, 633 (2000).
(31) L. Pauling, The Nature of the Chemical Bond (Cornell University Press, Ithaca, New York, 1960), Chap.3.

CUSTOMIZING
TO YOUR SPECIFIC NEEDS

Micro-manipulators, preparation materials, darkroom and general lab supplies, books, grids and apertures. Many items are manufactured in our machine shop, so customizing to your specific need is not a problem.

Some of the accessories and laboratory supplies we can supply are tweezers, tools, TEM CCD imaging systems, tensile testers, turbo evaporators, sputter coaters, substages, specimen holders, standards, carbon coaters, and more...

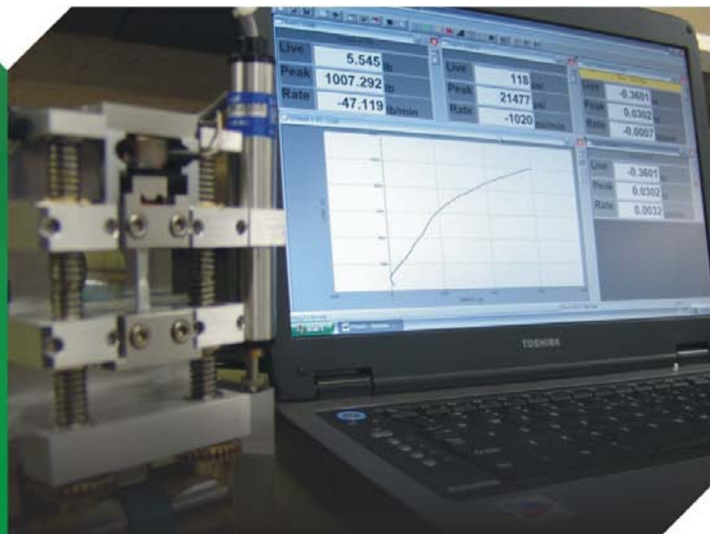

ERNEST F. FULLAM, INC.
Microscopy & Laboratory Supplies

900 Albany Shaker Road
Latham NY 12110 - 1491

Tel: 518.785.5533 / Fax: 518.785.8647

sales@fullam.com
www.fullam.com

https://doi.org/10.1017/S1551929500054250 Published online by Cambridge University Press